ACS APPLIED MATERIALS & INTERFACES

Research Article

www.acsami.org

# Hysteretic Behavior upon Light Soaking in Perovskite Solar Cells Prepared via Modified Vapor-Assisted Solution Process

Chong Liu, Jiandong Fan,* Xing Zhang, Yanjiao Shen, Lin Yang, and Yaohua Mai*

College of Physics Science and Technology, Hebei University, Baoding, 071002, China

Supporting Information

**ABSTRACT:** Recently, the organic−inorganic hybrid perovskite solar cells exhibit rapidly rising efficiencies, while anomalous hysteresis in perovskite solar cells remains unsolvable. Herein, a high-quality perovskite thin film is prepared by a modified vapor-assisted solution process, which is a simple but well-controllable method proven to be capable of producing a thin film with full surface coverage and grain size up to micrometers. The as-fabricated perovskite solar cell has efficiency as high as 10.2%. The hysteresis effects of both planar and mesoscopic $TiO_2$-based perovskite solar cells have been comprehensively studied upon illumination. The results demonstrate that mesoporous-based perovskite cells combined with remarkable grain size are subject to alleviating the hysteresis effects in comparison to the planar cells. Likewise, mesoscopic $TiO_2$-based perovskite cells perform independently of illumination and bias conditions prior to the measurements, whereas the planar cells display a reversible behavior of illumination and applied bias-dependent I−V curves. The present study would refer strip road for the stability study of the perovskite solar cells.

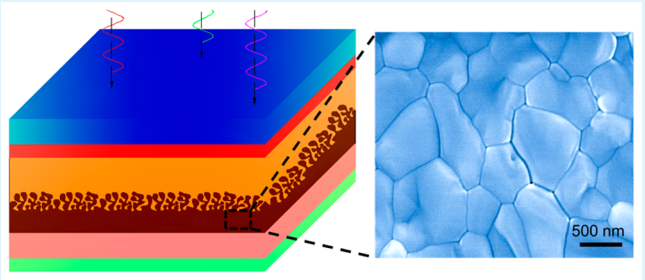


**KEYWORDS:** *perovskite solar cells, vapor-assisted solution process, hysteresis, light soaking, polarization*

## INTRODUCTION

Methylammonium lead halide perovskite solar cells have attracted considerable attention due to their high efficiency that has been improved rapidly during the past 5 years.[1−8] The outstanding advantages of such solar cells including low cost, flexibility, easy preparation, and large charge-carrier diffusion length would facilitate it toward scaling up to production levels.[9] Recently, the lack of understanding fundamental principle provokes much attention to various approaches, for instance, transient photovoltage and photocurrent,[10] impedance spectroscopy,[11,12] femtosecond transient optical spectroscopy,[13,14] and theoretical calculation.[15,16] The mechanism is likely to be continually ascertained in parallel with achieving high efficiency. Nevertheless, despite the superb properties, perovskite solar cells suffer from some weak points: (i) They are instable against humidity and UV light. The most commonly employed perovskite materials ($CH_3NH_3PbI_3$) are extremely sensitive to water vapor, which reacts to break down the crystal structure and dissolves the saltlike perovskite.[17,18] (ii) The lead element widely used in perovskite solar cells is toxic and could leach out of the solar panel onto rooftops or the soil below. Aside from those, perovskite solar cells struggle with a strong hysteresis in current−voltage (I−V) measurements, which was pointed out by Henry Snaith in early 2014.[19] A large discrepancy between the forward scan (here, we define the forward scan direction from short circuit to forward bias (SC-FB)) and reverse scan (we define the reverse scan direction from forward bias to short circuit (FB-SC)) was associated with the anomalous hysteresis, which results in a considerable error in evaluating the real efficiency. The anomalous hysteresis behavior in perovskite solar cells inhibits its stabilized power output under working conditions. However, little attempt has been performed to elucidate the physical mechanism and finally resolve the hysteresis in perovskite solar cells. Snaith hypothesized three possible origins of the effect: (i) Defect density within or near the surface of the perovskite absorbers or specifically generated interface states. (ii) A slow polarization of the material may occur since the ferroelectric properties of organometal trihalide perovskites. (iii) The interstitial ions would be able to aid the charge collection under working conditions. Park and co-worker described the hysteresis effects in view of perovskite grain size and the presence or absence of a mesoscopic $TiO_2$ layer.[20] Also, such transient process was also found to be consistent with a polarization response of the perovskite absorbers, which gives rise to hysteretic behavior.[21] In any case, more studies are still needed to understand the reason that results in the hysteretic effects in perovskite solar cells.

Apart from the hysteresis behavior, it is well-known that termed light soaking was employed to enhance the performance of both dye-sensitized and organic solar cells.[22,23] The architecture and composition of perovskite solar cells are similar to dye-sensitized solar cells and/or organic solar cells. Its photovoltaic properties are thereby likely to be affected by

Received: January 13, 2015
Accepted: April 10, 2015
Published: April 10, 2015





DOI: 10.1021/acsami.5b00375
ACS Appl. Mater. Interfaces 2015, 7, 9066−9071

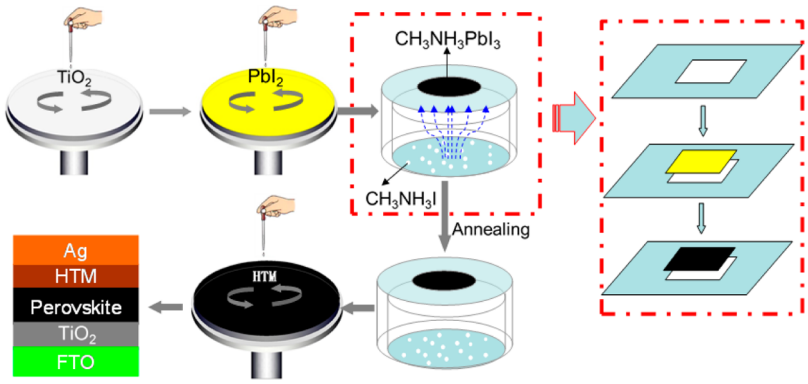


**Figure 1.** Schematic illustration of the procedure of perovskite solar cells prepared via modified VASP.

termed light soaking. In this scenario, the effect of light soaking on photovoltaic performance allows extending the hysteresis phenomenon and giving a potential explanation. However, little attention is paid to the dependence of performance of perovsikte solar cell on light soaking, particularly the hysteretic behavior evolution upon light soaking in perovskite solar cells.[21]

In this study, we have employed a modified vapor-assisted solution process (VASP) to fabricate both planar and mesoscopic perovskite solar cells. A slight hysteresis behavior is observed in the present solar cell compared to the solution processed-based solar cell. Meanwhile, the I−V curves evolution upon light soaking under applied biases are systematically studied for planar and mesoscopic structure. On the basis of this, we propose a potential mechanism that gives rise to the hysteresis effect.

## EXPERIMENTAL SECTION

**Thin Film and Solar Cell Fabrication.** Fluorine doped tin oxide (FTO)-coated glass (8 Ω/□, Nippon) was cut with 25 mm length and 25 mm width. The glass was cleaned with deionized water, acetone, and alcohol by turn, then dried by $N_2$, and finally treated under oxygen plasma for 3 min. A 50 nm thick compact layer of $TiO_2$ was then deposited on the FTO glass using titanium precursor liquid and sintered for 30 min at 500 °C.[24] The titanium precursor liquid was prepared by pipetting a mixed solution of 2.5 mL anhydrous ethanol and 35 μL HCl (2 M) into another mixed solution of 2.5 mL anhydrous ethanol and 350 μL titanium isopropoxide. For the mesoscopic cells, the mesoscopic $TiO_2$ layers were deposited by spin coating at 5000 rpm for 30 s using a commercial $TiO_2$ paste (Dyesol 18NRT, Dyesol) diluted in anhydrous ethanol (1:3.5 by weight). After drying at 125 °C, the substrate was sintered for 30 min at 500 °C. Afterward, $PbI_2$ (Aladdin) solution was prepared in DMF (Aladdin) at the concentration of 426 mg/mL. The prepared $PbI_2$ solution was preheated at 110 °C on a hot plate, followed by spin coating on the substrates at 2000 rpm for 30 s and then put back on the hot plate for 15 min of drying. A set of culture dishes were used to fix the $PbI_2$ substrates, which faced the spread $CH_3NH_3I$ powder at a suitable distance (Figure 1). To obtain the perovskite thin film, the culture dishes were then put into a tube furnace at 150 °C for 4 h. After cooling down to room temperature, the perovskite films were washed by isopropanol and annealed for 1 h at 150 °C. For the planar cells, the $PbI_2$ solution was directly spin-coated on the $TiO_2$ compact layers instead of mesoscopic $TiO_2$ layers; the followed procedures were the same as mesoscopic cells. The hole-transport material (HTM) solution was spin-coated on the substrates at 2000 rpm for 30 s by a mixed solution including a spiro-OMeTAD (72.3 mg/mL), 17.5 μL of Libis (trifluoromethanesulfonyl) imide (Li-TFSI, Sigma) in acetonitrile (520 mg/mL), and 28.8 μL of *tert*-butylpyridine (tBP, Sigma). Ag (100 nm) was thermally evaporated on top of the device to form the back contact after leaving the prepared cells in a desiccator for 8 h.

**Characterization.** X-ray diffraction (XRD) patterns were obtained with Cu Kα ($\lambda$ = 1.5406 Å) radiation in a reflection geometry on a Bruker D8 operating at 40 kV and 40 mA. Field-emission scanning electron microscopy (FESEM) was used to characterize the morphology of the obtained substrates. Both top-down and cross-sectional views were obtained using a JEOL JSM-7500F. Current−voltage (J−V) characteristics of perovskite solar cells were measured using a semiconductor device analyzer (Agilent B1500A) and a Newport solar simulator (XES-200S1) with AM 1.5 G spectral distributions. The illumination power at the sample was adjusted to 1000 W $m^{-2}$ using a certified reference solar cell (PVM956). The active area of solar cell was controlled to be 7.065 $mm^2$.

## RESULTS AND DISCUSSION

The VASP allowed obtaining perovskite films with full surface coverage, uniform grain structure with grain size up to micrometers, and 100% precursor transformation completeness.[25] Herein, we have modified the VASP and employed a set of culture dishes to fix the $PbI_2$ substrate, which faced down to $CH_3NH_3I$ powder (Figure 1). The bottom-up evaporated $CH_3NH_3I$ facilitates the crystallization of perovskite with full surface coverage and uniform grain structure with remarkable grain size up to microscale, which far outweighs the solution-processed perovskite thin film (Figure 2a,b and Figure S1, Supporting Information). The controllable kinetic reactivity of $CH_3NH_3I$ and $PbI_2$ as well as the thermodynamic stability of perovskite during the in situ growth process provides an efficient way to scale up the perovskite thin film for commercial application.

The XRD pattern (Figure S2, Supporting Information) clearly displays that the film is composed of the pure perovskite phase with orthorhombic structure (14.1°, 28.4°, and 31.9°). It should be mentioned that $PbI_2$ peak located at 12.7° can also be detected in the perovskite thin film after annealing. The presence of $PbI_2$ species in the grain boundaries upon thermal annealing was considered to result in a successful passivation that controls the carrier behavior along the heterojunctions. This type I band alignment between $PbI_2$ and perovskite forms


DOI: 10.1021/acsami.5b00375
ACS Appl. Mater. Interfaces 2015, 7, 9066−9071

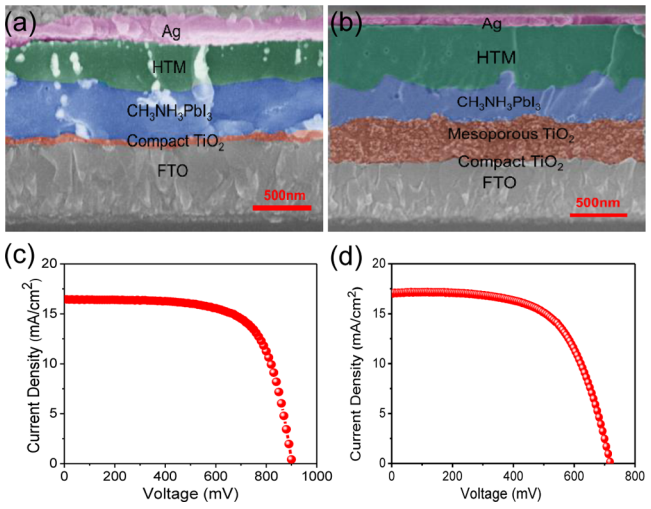


**Figure 2.** Cross-sectional SEM images of perovskite solar cells: (a) planar structure and (b) mesoscopic structure; (c) I–V curve of planar-structured solar cell; (d) I–V curve of mesoscopic structured solar cell.

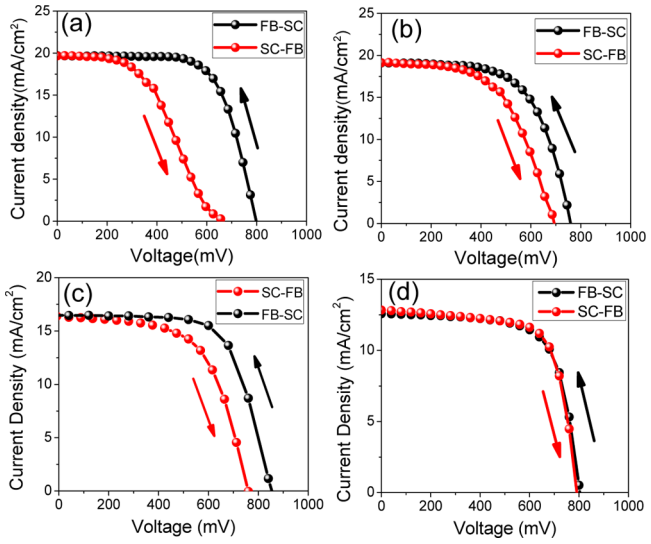


**Figure 3.** Influence of solar cell architecture upon current–voltage hysteresis. Forward bias to short circuit (FB-SC) and short circuit to forward bias (SC-FB) current–voltage curves measured under simulated AM 1.5 100 mW $cm^{-2}$ sunlight for (a) solution-processed planar-structured $TiO_2$-based solar cell, (b) solution-processed mesoscopic $TiO_2$-based solar cell, (c) vapor-assisted planar-structured $TiO_2$-based solar cell, and (d) vapor-assisted mesoscopic $TiO_2$-based solar cell.

energy barriers to prevent excitons from the surface defects and traps states.[26]

Figure 2a,b and Figure S1 demonstrate the cross-sectional and top-down SEM images of perovskite solar cell with planar and mesoscopic structure, respectively. Clearly, the full surface coverage, microscale grain size, and uniform grain structure of the as-obtained perovskite film can effectively avoid the recombination of photogenerated electrons and holes. The corresponding record photovoltaic performances of planar perovskite solar cells are $J_{SC}$ = 16.5 mA/cm$^2$, $V_{OC}$ = 0.9 V, fill factor (FF) = 68.9%, and power conversion efficiency (PCE) = 10.2%, whereas the mesoporous one is $J_{SC}$ = 17.0 mA/cm$^2$, $V_{OC}$ = 0.7 V, FF = 62.5%, and PCE = 7.7%. Relatively lower $V_{OC}$ for the mesoscopic cells compared to the planar ones was obtained while $J_{SC}$ and FF remained similar. It might be attributed to the density of perovskite thin films, while the planar $TiO_2$ layer promotes the perovskite thin film toward compact crystal morphology (Figure S1, Supporting Information). Similar phenomena were also observed by Park and co-worker.[20] They found that dark current decreased with decreasing the size in perovskite thin film, which indicated that the enhancement of $V_{OC}$ with relatively small crystal size was caused by its compact crystal morphology preventing hole-transport materials from direct contact with electron transport layer, i.e., $TiO_2$ and FTO. With respect to the hysteretic behavior upon light soaking for both cases, further characterizations and discussions will be performed afterward.

Hysteresis effects can be observed for a variety of device architectures on $TiO_2$ planar and/or $TiO_2/Al_2O_3$ mesoscopic cells. As mentioned previously, hysteresis effects might be associated with the perovskite sizes, which are generally dependent on the growth condition of perovskite crystal. So far, no literature was reported regarding the hysteresis effects of perovskite solar cell prepared via VASP. We compared the hysteresis effects of solution-processed perovskite solar cells with the cells by modified VASP. Figure 3 shows the influence of solar cell architecture upon current–voltage hysteresis effects.

Here, we quantified the hysteresis effect in the I–V curve; a modified I–V hysteresis index (HI) is defined by eq 1,[27]

$$\mathrm{HI} = \frac{J_{\text{FB-SC}}(3V_{OC}/5) - J_{\text{SC-FB}}(3V_{OC}/5)}{J_{\text{FB-SC}}(3V_{OC}/5)} \quad (1)$$

where $J_{\text{FB-SC}}$ $(3V_{OC}/5)$ and $J_{\text{SC-FB}}$ $(3V_{OC}/5)$ represent photocurrent density at 60% of $V_{OC}$ for the scan of FB-SC and SC-FB, respectively. A HI of 0 represents a cell without hysteresis, while a HI of 1 corresponds to the case that the hysteresis is as high as the magnitude of the photocurrent.

Parts (a) and (b) of Figure 3 demonstrate the hysteresis effects of solution-processed planar and mesoscopic $TiO_2$-based solar cells, respectively. Compared with the planar structure without mesoscopic $TiO_2$ layer, no significant difference in I–V curves between FB-SC and SC-FB is observed for the mesostructured device with mesoscopic $TiO_2$ layer (HI = 0.06), whereas severe I–V hysteresis is observed for the planar structure (HI = 0.23). This suggests that the presence of mesoscopic $TiO_2$ layer alleviates the hysteresis effects. Parts (c) and (d) of Figure 3 display the hysteresis effects of planar and mesoscopic $TiO_2$-based solar cells by modified VASP, respectively. The corresponding HI is 0.05 and 0.01, respectively. Obviously, the hysteresis effects have been significantly relieved compared with those of the solution-processed solar cells. This might be associated with the crystallization size of perovskite (Figure S1, Supporting Information); a remarkable grain size up to microscale without grain boundary does not require longer time to reach the steady-state photocurrent. It is suggested that the relaxation time of dipole alignment and/or the extent of developed aligned dipole in perovskite thin film is significantly influenced by crystal size, which in turn directly affects the I–V hysteresis.[20] In both cases, the hysteresis effects are relatively severe in the case of a planar heterojunction in comparison to mesoscopic $TiO_2$-based solar cells. Similar observations were also obtained for the solution-processed solar cells elsewhere.[20,27,28] It is well-known that the organometal trihalide


DOI: 10.1021/acsami.5b00375
ACS Appl. Mater. Interfaces 2015, 7, 9066–9071

perovskites have ferroelectric properties, which will give rise to a slow polarization upon applied biases.[29,30] These behaviors of perovskite solar cells might be associated with the large diffusion capacitance of the cells operating under reverse or forward biases.[31] As shown in Figure 4a,c, under reverse biases,

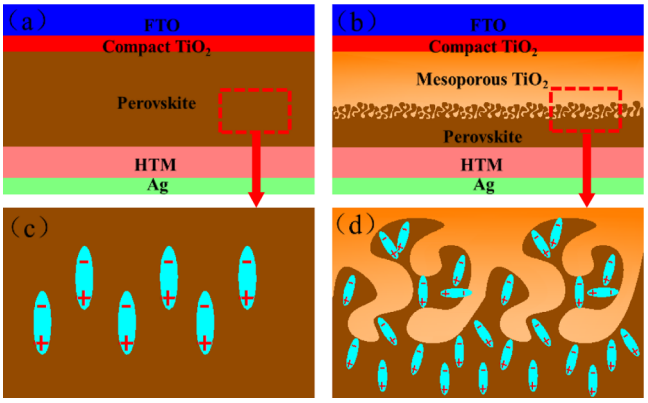


**Figure 4.** Schematic mechanism illustration of the polarization in (a) planar-structured solar cell and (b) mesoporous-structured solar cell under reverse biases; (c) and (d) are the magnified images of the corresponding regions in (a) and (b), respectively.

an internal electric field that is opposite to the direction of external electric field may remain due to an ordered array of dipoles when the ferroelectricity of the perovskite thin film is sufficiently large. The remnant polarization is supposed to suppress the flow of photocurrent since the direction of internal electric field is opposite to the photocurrent. In the case of mesoscopic $TiO_2$-based solar cells, a disorder dipoles array can be developed where ferroelectric domains of perovskite are weakened as shown in Figure 4b,d. Hysteresis effects can thereby be suppressed when most perovskites are confined in the mesoscopic $TiO_2$ with the presence of a thin capping layer, avoiding the short circuit between the electron-transport layer ($TiO_2$) and hole-transport layer (spiro-OMeTAD). To further elucidate the effect of mesoscopic $TiO_2$ layer on the hysteresis effects of perovskite solar cells, we verified the layer thickness of mesoporous $TiO_2$ and checked the hysteretic trend with thickness. As shown in Figure S3, it clearly demonstrates that the hysteresis effects are reducing with the mesoporous $TiO_2$ thickness increasing from 0 to 350 nm. This trend is consistent with a previous report,[20] and further confirms that the degree of hysteresis tends to diminish as the size of perovskite and mesoporous $TiO_2$ layer thickness increases.

It was proven that termed light soaking prior to the I–V measurement has a significant influence on the solution-processed perovskite solar cells.[21] To rule out the possibility of light-soaking-induced structural variation, we have comprehensively explored the effect of termed light soaking on the structure of perovskite thin film prepared via modified VASP with an aim of finally figuring out the light-soaking-dependent hysteresis behavior under applied biases in the perovskite solar cells. XRD patterns show that the crystal structure remains exactly the same while the as-prepared perovskite thin film was exposed upon illumination for 1 h (Figure S2, Supporting Information). It turns out that the perovskite thin films did not change their crystallography structure by simply light soaking.

Again, the photovoltaic performances of dye-sensitized, polymer, and perovskite solar cells have been proven to be enhanced with termed light soaking.[21−23] Heretofore, there has been no discussion with respect to the effect and importance of preillumination steps for VASP-prepared perovskite cells. We have systematically studied the evolution of the I–V curve with modified VASP-prepared perovskite cells upon light soaking at forward and reverse biases conditions, respectively. It is supposed to be affected by cycling the device under illumination several times under applied biases prior to performing the I–V measurement. Figure 5a,b exhibits the

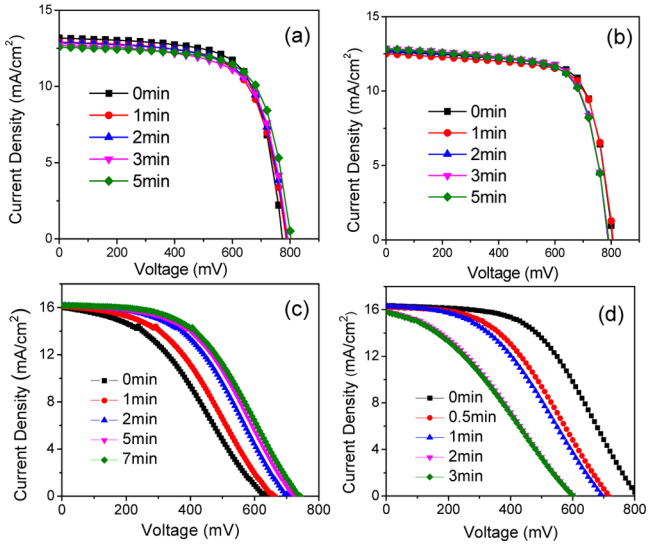


**Figure 5.** Evolution of current–voltage curves upon light soaking. Vapor-assisted mesoscopic $TiO_2$-based solar cells under (a) forward bias and (b) reverse bias. Vapor-assisted planar-structured $TiO_2$-based solar cells under (c) forward bias and (d) reverse bias.

evolution of I–V curves with modified VASP-prepared mesoscopic $TiO_2$-based solar cells measured at forward and reverse biases upon illumination. As expected, the I–V curves stay almost the same with cycling illumination under forward and reverse biases. In contrast, parts (c) and (d) of Figure 5 reveal the corresponding cases of planar structure solar cells under forward and reverse biases, respectively. Figure S4 clearly displays the photovoltaic performance trends as a function of light-soaking time under applied biases. It turns out that the light soaking under forward bias conditions dramatically improves FF and $V_{OC}$, which leads to a power conversion efficiency increase by a factor 1.5. Illumination under reverse bias, where the external electric field is in the opposite direction, has the opposite effect that decreases FF and $V_{OC}$ intensely. From the discussions above, it is clear that the remnant polarization is supposed to suppress the flow of photocurrent under reverse bias conditions. The FF and $V_{OC}$ would be sacrificed by cycling the device upon illumination under reverse bias conditions in which the remnant polarized charges screen the electric field. In contrast, the remnant polarized field introduced by the forward bias has the same direction as the electric field, which aids the separation and transport of the photogenerated charge carriers. Consequently, the FF and $V_{OC}$ have been improved by cycling the device upon illumination under forward bias conditions. Meanwhile, all of the processes are reversible by cycling the voltage bias conditions during light soaking. Similar behavior was also observed in the solution-processed perovskite solar cell.[21] The repeatable process may be attributed to the ferroelectric polarization effect inside perovskite film where the relaxation/


DOI: 10.1021/acsami.5b00375
ACS Appl. Mater. Interfaces 2015, 7, 9066−9071

arrangement of dipoles array may occur under forward/reverse bias conditions upon illumination. Additionally, by contrasting the light-soaking-dependent I–V behavior of mesoscopic and planar structure, the former performed fairly independently of illumination and/or bias conditions prior to the measurements (Figure 5). This further certifies that the mesoscopic structure cells are subject to alleviating the hysteresis effects in comparison to the planar cells, where the direction of electrons flow is against the internal electric field induced by order of dipoles arrangement. It is also worthy of note that the initial transient photocurrent has been quenched at applied bias upon continued illumination in the case of planar structure cells rather than the mesoscopic structure, which might be associated with the hysteresis effects induced by the dipoles polarization of perovskite film under applied bias upon illumination. Further studies are underway to determine the mechanisms of hysteresis effects in perovskite solar cells.

## CONCLUSIONS

We demonstrate a modified VASP to prepare high-quality perovskite thin films with uniform grain structure. The solar cell derived from the as-prepared perovskite thin film displays a PCE of 10.2%. In comparison to the solution-processed perovskite solar cells, the as-fabricated cells by the present method have been proven to exhibit slight hysteresis effects due to the remarkable grain size up to microscale without grain boundary that does not require longer time to reach the steady-state photocurrent. The study of hysteretic behavior upon light soaking in perovskite solar cells further confirms that the mesoscopic $TiO_2$-based electron-transport layer are supposed to relieve the hysteresis effects in comparison to the planar cells in which the remnant polarization may suppress the flow of photocurrent. This study provides a potential approach to pave the way for exploring the stability of perovskite solar cells.

## ASSOCIATED CONTENT

### Supporting Information

Top-down SEM images of perovskite thin films prepared by solution-processed method and modified VASP and XRD patterns of perovskite thin film upon illumination with different times, the I–V evolution of perovskite solar cells as a function of mesoporous $TiO_2$ thickness, and the photovoltaic performances trend as a function of light-soaking time under applied biases. This material is available free of charge via the Internet http://pubs.acs.org.

## AUTHOR INFORMATION

### Corresponding Authors

*Phone: +86 312 5077382. Fax: +86 312 5077382. E-mail: jdfan@hbu.edu.cn (J.F.).

*E-mail: yaohuamai@hbu.edu.cn (Y.M.).

### Notes

The authors declare no competing financial interest.

## ACKNOWLEDGMENTS

The research was funded by the "973 program" early projects (No. 2014CB260405), "Advanced Talents Program of Hebei Province (No. GCC2014013), Top Young Outstanding Innovative Talents Program of Hebei Province (No. BJ2014009), and Natural Science Foundation of Hebei Province (No. F2015201189). J. Fan is thankful for the support of "100 Talents Program of Hebei Province".

## REFERENCES

(1) Kojima, A.; Teshima, K.; Shirai, Y.; Miyasaka, T. Organometal Halide Perovskites as Visible-Light Sensitizers for Photovoltaic Cells. *J. Am. Chem. Soc.* **2009**, *131*, 6050–6051.

(2) Kim, H. S.; Lee, C. R.; Im, J. H.; Lee, K. B.; Moehl, T.; Marchioro, A.; Moon, S. J.; Humphry-Baker, R.; Yum, J. H.; Moser, J. E.; Grätzel, M.; Park, N. G. Lead Iodide Perovskite Sensitized All-Solid-State Submicron Thin Film Mesoscopic Solar Cell with Efficiency Exceeding 9%. *Sci. Rep.* **2012**, *2*, 591.

(3) Lee, M. M.; Teuscher, J.; Miyasaka, T.; Murakami, T. N.; Snaith, H. J. Efficient Hybrid Solar Cells Based on Meso-Superstructured Organometal Halide Perovskites. *Science* **2012**, *338*, 643–647.

(4) Burschka, J.; Pellet, N.; Moon, S. J.; Humphry-Baker, R.; Gao, P.; Nazeeruddin, M. K.; Grätzel, M. Sequential Deposition as a Route to High-Performance Perovskite-Sensitized Solar Cells. *Nature* **2013**, *499*, 316–319.

(5) Liu, M.; Johnston, M. B.; Snaith, H. J. Efficient Planar Heterojunction Perovskite Solar Cells by Vapour Deposition. *Nature* **2013**, *501*, 395–398.

(6) Mei, A.; Li, X.; Liu, L.; Ku, Z.; Liu, T.; Rong, Y.; Xu, M.; Hu, M.; Chen, J.; Yang, Y.; Grätzel, M.; Han, H. A Hole-Conductor–Free, Fully Printable Mesoscopic Perovskite Solar Cell with High Stability. *Science* **2014**, *345*, 295–298.

(7) Zhou, H.; Chen, Q.; Li, G.; Luo, S.; Song, T. b.; Duan, H. S.; Hong, Z.; You, J.; Liu, Y.; Yang, Y. Interface Engineering of Highly Efficient Perovskite Solar Cells. *Science* **2014**, *345*, 542–546.

(8) Fan, J.; Jia, B.; Gu, M. Perovskite-Based Low-Cost and High-Efficiency Hybrid Halide Solar Cells. *Photonics Res.* **2014**, *2*, 111–120.

(9) Seo, J.; Park, S.; Kim, Y. C.; Jeon, N. J.; Noh, J. H.; Yoon, S. C.; Seok, S. I. Benefits of Very Thin PCBM and LiF Layers for Solution-Processed p–i–n Perovskite Solar Cells. *Energy Environ. Sci.* **2014**, *7*, 2642–2646.

(10) Zhao, Y.; Zhu, K. Charge Transport and Recombination in Perovskite $(CH_3NH_3)PbI_3$ Sensitized $TiO_2$ Solar Cells. *J. Phys. Chem. Lett.* **2014**, *4*, 2880–2884.

(11) Dualeh, A.; Moehl, T.; Tétreault, N.; Teuscher, J.; Gao, P.; Nazeeruddin, M. K.; Grätzel, M. Impedance Spectroscopic Analysis of Lead-Iodide Perovskite-Sensitied Solid-State Solar Cells. *ACS Nano* **2014**, *8*, 362–373.

(12) Kim, H. S.; Mora-Sero, I.; Gonzalez-Pedro, V.; Fabregat-Santiago, F.; Juarez-Perez, E. J.; Park, N. G.; Bisquert, J. Mechanism of Carrier Accumulation in Perovskite Thin-Absorber Solar Cells. *Nat. Commun.* **2013**, *4*, 2242.

(13) Xing, G.; Mathews, N.; Sun, S.; Lim, S. S.; Lam, Y. M.; Grätzel, M.; Mhaisalkar, S.; Sum, T. C. Long-Range Balanced Electron-and Hole-Transport Lengths in Organic-Inorganic $CH_3NH_3PbI_3$. *Science* **2013**, *342*, 344–347.

(14) Stranks, S. D.; Eperon, G. E.; Grancini, G.; Menelaou, C.; Alcocer, M. J. P.; Leijtens, T.; Herz, L. M.; Petrozza, A.; Snaith, H. J. Electron-Hole Diffusion Lengths Exceeding 1 Micrometer in an Organometal Trihalide Perovskite Absorber. *Science* **2013**, *342*, 341–344.

(15) Edri, E.; Kirmayer, S.; Mukhopadhyay, S.; Gartsman, K.; Hodes, G.; Cahen, D. Elucidating the Charge Carrier Separation and Working Mechanism of $CH_3NH_3PbI_{3-x}Cl_x$ Perovskite Solar Cells. *Nat. Commun.* **2014**, *5*, 3461.

(16) Even, J.; Pedesseau, L.; Jancu, J. M.; Katan, C. Importance of Spin–Orbit Coupling in Hybrid Organic/Inorganic Perovskites for Photovoltaic Applications. *J. Phys. Chem. Lett.* **2013**, *4*, 2999–3005.

(17) Ito, S.; Tanaka, S.; Manabe, K.; Nishino, H. Effects of Surface Blocking Layer of $Sb_2S_3$ on Nanocrystalline $TiO_2$ for $CH_3NH_3PbI_3$ Perovskite Solar Cells. *J. Phys. Chem. C* **2014**, *118*, 16995–17000.

(18) Leijtens, T.; Eperon, G. E.; Pathak, S.; Abate, A.; Lee, M. M.; Snaith, H. J. Overcoming Ultraviolet Light Instability of Sensitized $TiO_2$ with Meso-Superstructured Organometal Tri-Halide Perovskite Solar Cells. *Nat. Commun.* **2014**, *4*, 2885.

(19) Snaith, H. J.; Abate, A.; Ball, J. M.; Eperon, G. E.; Leijtens, T.; Noel, N. K.; Stranks, S. D.; Wang, J. T. W.; Wojciechowski, K.; Zhang,



DOI: 10.1021/acsami.5b00375
*ACS Appl. Mater. Interfaces* 2015, 7, 9066–9071

W. Anomalous Hysteresis in Perovskite Solar Cells. *J. Phys. Chem. Lett.* **2014**, *5*, 1511−1515.
(20) Kim, H. S.; Park, N. G. Parameters Affecting I−V Hysteresis of $CH_3NH_3PbI_3$ Perovskite Solar Cells: Effects of Perovskite Crystal Size and Mesoporous $TiO_2$ Layer. *J. Phys. Chem. Lett.* **2014**, *5*, 2927−2934.
(21) Unger, E. L.; Hoke, E. T.; Bailie, C. D.; Nguyen, W. H.; Bowring, A. R.; Heumüller, T.; Christoforod, M. G.; McGehee, M. D. Hysteresis and Transient Behavior in Current-Voltage Measurements of Hybrid-Perovskite Solar Cells. *Energy Environ. Sci.* **2014**, *7*, 3690−3698.
(22) Yang, L.; Xu, B.; Bi, D.; Tian, H.; Boschloo, G.; Sun, L.; Hagfeldt, A.; Johansson, E. M. J. Initial Light Soaking Treatment Enables Hole Transport Material to Outperform Spiro-OMeTAD in Solid-State Dye-Sensitized Solar Cells. *J. Am. Chem. Soc.* **2013**, *135*, 7378−7385.
(23) Sista, S.; Park, M. H.; Hong, Z.; Wu, Y.; Hou, J.; Kwan, W. L.; Li, G.; Yang, Y. Highly Efficient Tandem Polymer Photovoltaic Cells. *Adv. Mater.* **2010**, *22*, 380−383.
(24) Ball, J. M.; Lee, M. M.; Hey, A.; Snaith, H. J. Low-Temperature Processed Meso-Superstructured to Thin-Film Perovskite Solar Cells. *Energy Environ. Sci.* **2013**, *6*, 1739−1743.
(25) Chen, Q.; Zhou, H.; Hong, Z.; Luo, S.; Duan, H. S.; Wang, H. H.; Liu, Y. S.; Li, G.; Yang, Y. Planar Heterojunction Perovskite Solar Cells Via Vapor-Assisted Solution Process. *J. Am. Chem. Soc.* **2014**, *136*, 622−625.
(26) Chen, Q.; Zhou, H.; Song, T.-B.; Luo, S.; Hong, Z.; Duan, H. S.; Dou, L.; Liu, Y. S.; Yang, Y. Controllable Self-Induced Passivation of Hybrid Lead Iodide Perovskites toward High Performance Solar Cells. *Nano Lett.* **2014**, *14*, 4158−4163.
(27) Sanchez, R. S.; Gonzalez-Pedro, V.; Lee, J. W.; Park, N. G.; Kang, Y. S.; Mora-Sero, I.; Bisquert, J. Slow Dynamic Processes in Lead Halide Perovskite Solar Cells. Characteristic Times and Hysteresis. *J. Phys. Chem. Lett.* **2014**, *5*, 2357−2363.
(28) Chen, H. W.; Sakai, N.; Ikegami, M.; Miyasaka, T. Emergence of Hysteresis and Transient Ferroelectric Response in Organo-Lead Halide Perovskite Solar Cells. *J. Phys. Chem. Lett.* **2015**, *6*, 164−169.
(29) Stoumpos, C. C.; Malliakas, C. D.; Kanatzidis, M. G. Semiconducting Tin and Lead Iodide Perovskites with Organic Cations: Phase Transitions, High Mobilities, and Near-Infrared Photoluminescent Properties. *Inorg. Chem.* **2013**, *52*, 9019−9038.
(30) Kutes, Y.; Ye, L.; Zhou, Y.; Pang, S.; Huey, B. D.; Padture, N. P. Direct Observation of Ferroelectric Domains in Solution-Processed $CH_3NH_3PbI_3$ Perovskite Thin Films. *J. Phys. Chem. Lett.* **2014**, *5*, 3335−3339.
(31) Koide, N.; Han, I. Measuring Methods of Cell Performance of Dye-Sensitized Solar Cells. *Rev. Sci. Instrum.* **2004**, *75*, 2828−2831.


DOI: 10.1021/acsami.5b00375
*ACS Appl. Mater. Interfaces* 2015, 7, 9066−9071